Temperature responsive poly(trimethylene carbonate)-*block*-poly(L-glutamic acid) copolymer: polymersomes fusion and fission

C. Sanson,[ab] J.-F. Le Meins,[ab] C. Schatz,[ab] A. Soum[ab] and S. Lecommandoux*[ab]

Received 24th November 2009, Accepted 2nd February 2010
First published as an Advance Article on the web 3rd March 2010
DOI: 10.1039/b924617g

We have reported on a new type of thermotropic transition in synthetic diblock copolymer vesicles. Vesicles were self-assembled from a well-defined poly(trimethylene carbonate)-*b*-poly(L-glutamic acid) ($PTMC_{22}$-*b*-PGA_{14}, $M_n = 4.05*10^3$ g mol^{-1}) copolymer. $PTMC_{22}$ is a semi-crystalline hydrophobic block with a melting endotherm observed at 37 °C in the bulk copolymer and at 34–35 °C in the vesicular dispersions. This temperature transition, as observed by μDSC in the aqueous vesicular dispersions, arose from a variation of the PTMC chain packing inside the vesicular bilayer. A large range of vesicle sizes, from 100 nm to 5 μm, was accessible by varying the experimental conditions to prepare the vesicles. Large vesicles were more sensitive to the melting transition due to a low membrane curvature and high hydrophobic block interactions. By many aspects, this transition presented strong analogies with the gel-to-liquid crystalline phase transition observed in liposomes. Vesicle budding and fission occurred when temperature was increased above the PTMC melting temperature and fusion events were observed when temperature was decreased. The fission process was certainly due to the creation of an excess area upon heating whereas fusion is due to membrane defects arising from variation in PTMC membrane packing. As a consequence, the size of the vesicles was found correlated to the crystalline state of the PTMC chains, its variation being fully reversible with the temperature.

I. Introduction

Polymer vesicles are attractive structures designed to mimic biosystems such as living cells or viruses due to their intrinsic nature of closed interface between an inner and an outer medium. This vesicular structure can be compared to a viral capsid due to its ability to carry, target and release drugs in a controlled manner, similar in the principle to how viruses deliver their nucleic acids within cells.[1,2] The formation of synthetic polymer vesicles is well-documented and it is usually accepted that an amphiphilic block copolymer with an hydrophilic to hydrophobic weight ratio of (35 ± 10)% forms preferentially vesicles over spherical micelles.[3] Using the versatility of block copolymer chemistry (chemical composition, block lengths, copolymer molar mass), characteristics and properties of the vesicle surface can be tuned to achieve cell-like functions such as molecular transport, barrier formation, templating and signaling.[4,5] In this perspective, the modification of the membrane physical properties has been assessed. As an example, the stability of the membrane has been varied by crosslinking poly(ethylene oxide)-*b*-polybutadiene (PEO-*b*-PBD)[6] and poly(L-glutamic acid)-*b*-polybutadiene (PGA-*b*-PBD)[7] polymersome membranes and its elasticity modulated by mixing PEO-*b*-PBD and poly(ethylene oxide)-*b*-poly(ethyl ethylene) (PEO-*b*-PEE).[6] Also, control of degradability has been achieved by blending poly(ethylene oxide)-*b*-polylactide (PEO-*b*-PLA) or poly(ethylene oxide)-*b*-poly(ε-caprolactone) (PEO-*b*-PCL) with crosslinked PEO-*b*-PBD.[8,9] Recent studies also focused on the integration of proteins into membranes to mimic the heterogeneity of cell membranes which are complex assemblies of lipids, glycolipids, membrane proteins and glycoproteins. In this approach, incorporation of channel proteins allowed a specific and reversible exchange through synthetic membranes[10–12] leading to nanoreactors used for calcium biomineralization,[13] water permeation enhancement[10] or even DNA injection by a virus assisted process.[14] Polymersomes also offer a tremendous interest as multifunctional nanocarriers used for diagnosis and therapy by incorporating soluble and insoluble drugs and imaging probes.[15–19]

Maximum therapeutic efficiency of the substances encapsulated in the aggregates requires the ability to control the release. To address this goal, strategies have been developed in which a specific stimulus (temperature, pH, light, oxidative environment…) destabilises the vesicular structure.[20–23]

Concerning thermosensitive polymersomes, responsiveness is achieved by using either a block presenting a critical solubility temperature (LCST or USCT)[24,25] or by using the change in secondary conformation of a polypeptide block.[26,27]

In natural vesicular systems assembled from phospholipids (liposomes), the temperature responsiveness is provided by the crystalline nature of the hydrophobic alkyl chains. Consequently, lipidic membranes, due to their liquid crystalline state of matter, exhibit a range of thermotropic transitions with a main phase transition indifferently named the chain-melting transition or the gel-to-liquid-crystalline phase transition. In most of liposomes, generally composed of saturated identical-chain phospholipids, the main transition occurs at a precise temperature

[a]*Université de Bordeaux, ENSCPB, 16 avenue Pey Berland, 33607 Pessac Cedex, France*
[b]*CNRS, Laboratoire de Chimie des Polymères Organiques, UMR5629, Pessac, France. E-mail: lecommandoux@enscbp.fr*

(T_m) depending on the alkyl chain length and the nature of the hydrophilic moiety.[28] The transition from an ordered gel phase (below T_m) to a disordered liquid crystalline phase (above T_m) results directly from the melting and reorganization of phospholipid hydrophobic alkyl chains inside the vesicular membrane. This membrane transition has proved to be useful for controlled drug delivery applications since permeability and release kinetics are maximal at the phase transition temperature.[29–31]

Concerning synthetic polymer systems, different studies have been conducted to assess the influence of block copolymer crystallization on the stability and properties of the resultant self-assembled structures. These studies first focused on the crystallization of crystalline-amorphous diblock copolymers with PEO as a crystalline block in organic solvent. For instance, annealing of a solution of polystyrene-*b*-poly(ethylene oxide) (PS-*b*-PEO) in cyclopentane above the PEO melting temperature and subsequent cooling down resulted in the formation of crystalline lamellar domains of poly(ethylene oxide) in between two brushes of solvated polystyrene.[32] Formation of PB-*b*-PEO superstructures in heptane were also reported and resulted from crystallization-induced aggregation of spherical micelles.[33] In addition, poly(ethylene)-*b*-poly(ethylene oxide) (PE-*b*-PEO) diblock copolymers have been evidenced to form spherical micelles with PE crystalline multicores in water.[34] PE melting temperature (32.6 °C) in the micellar cores was much lower than that of homopolymer (122.3 °C) due to the confined crystallization of PE in the nanodomains. These multicores in one micelle could reaggregate to a single-core as temperature increased. Recently, transition from spherical micelles to cylindrical micelles made of poly(ferrocenyldimethylsilane)-*b*-poly(2-vinylpyridine) (PFS-*b*-P2VP) was established in ethanol as the system ages. Evidence was provided that the crystallization of the PFS core polymer is the main driving force for the formation of the cylindrical morphologies.[35] All these results confirm that confinement of a crystallizable block in the core of self-assembled objects can modulate the crystalline physical properties and that crystallization/melting transition can induce aggregation or shape transformation of these objects.

To our knowledge, very few studies have been conducted on crystallization in vesicular membranes, the only relevant report concerning PEO-*b*-PCL based polymersomes which display first order phase transition upon heating as observed by calorimetry.[36] However, the consequences of this transition on the vesicle structure and properties were not explored.

We report here on the temperature induced crystallization/melting in synthetic poly(trimethylene carbonate)-*b*-poly(L-glutamic acid) (PTMC-*b*-PGA) vesicles in water. We demonstrate that the thermally controlled transition of the confined PTMC in the polymersome membrane bilayer depends mainly on membrane curvature (vesicle size). We studied the influence of vesicle size on the transition mechanism. All along this work, we highlight the strong similarities of this process with the main phase transition observed in liposomes. Thus, the present study is of interest not only for the development of novel type of thermosensitive polymersomes but also for its fundamental aspects due to the obvious analogies with lipidic vesicles.

II. Experimental

A. Materials

$PTMC_{22}$-*b*-PGA_{14} diblock copolymer was synthesized by ROP of γ-benzyl-L-glutamate *N*-carboxyanhydride initiated by a primary amine end-functionalized PTMC macroinitiator according to a previously described method.[37,38] All the experiments have been conducted on $PTMC_{22}$-*b*-PGA_{14} diblock copolymer (4050 g mol^{-1}) which presents a hydrophilic weight fraction of 44 wt% and a polydispersity index of 1.1. Laurdan, Nile Red and tris(hydroxymethyl)aminomethane (Tris) were purchased from Sigma and Bodipy FL from Molecular Probes and were used as received. Solvents for nanoprecipitation (DMSO, THF, MeOH) were used without prior purification.

B. Methods

As evidenced in a previous report,[37] by varying the conditions of nanoprecipitation (order of addition, choice of organic solvent and duration of addition) we were able to form PTMC-*b*-PGA vesicles with controlled sizes (ranging from 100 nm to a few microns) and narrow dispersities. The vesicular morphology was evidenced combining light and neutron scattering together with TEM imaging. In this study we have increased the accessible vesicular size range by playing also with copolymer concentration.

Typical preparation of block copolymer vesicles. In the methods detailed below, the term buffer designates a Tris buffer at pH 7.4.

Direct dissolution. $PTMC_{22}$-*b*-PGA_{14} (10 mg) was immersed in buffer (10 ml, 50 mM) at 50 °C under stirring. After 1 h, a bluish solution (without solid objects) is obtained indicating the formation of nanometric objects. The colloidal dispersion was eventually filtered off 20 times through a polycarbonate filter (200 nm pore size, Nucleopore) at 25 °C in order to reduce and control the average vesicles size.

Solvent displacement method (nanoprecipitation).[37] Buffer (4.5 mL, 50 mM) is added dropwise to $PTMC_{22}$-*b*-PGA_{14} (5 mg or 50 mg) solubilised in DMSO or THF–MeOH (0.5 mL), under magnetic stirring, leading to a homogeneous dispersion of vesicles. The organic solvent, the concentration of copolymer, the order of addition (water in organic solvent or the opposite) and the injection flow rate were varied and led to the formation of vesicles varying in sizes but with always low size dispersity. Organic solvent is then removed by extensive dialysis against buffer (10 mM) solution at pH 7.4. The different nanoprecipitation conditions and the corresponding sample codes are summarized in Table 1.

Characterization of $PTMC_{22}$-*b*-PGA_{14} dispersions

Dynamic light scattering. (DLS) experiments were performed using an ALV Laser goniometer, which consisted of a 35 mW HeNe linear polarized laser with a wavelength of 632.8 nm and an ALV-5000/EPP Multiple Tau Digital correlator with 125 ns initial sampling time. The accessible scattering angle range is from 40 up to 150°. However, most of the measurements were carried out at 90°. Aliquots of the samples (1 mL in a 1 cm diameter cylindrical glass cells) were immersed in a filtered

Table 1 Summary of methods used for vesicle formation ($T = 25$ °C) and the resultant hydrodynamic radii obtained

					Organic solvent		Injection duration	
Sample Code	$[copolymer]_{final}$/mg ml^{-1}	R_H/nm	Water in organic	Organic in water	DMSO	THF–MeOH	15 min	120 min
TW15	1	56		*		*	*	
WD15	1	95	*		*		*	
WT120-1 mg mL^{-1}	1	450	*			*		*
WT120-10 mg mL^{-1}	10	5000	*			*		*
DD	1	240	—	—	—	—	—	—

toluene bath. The samples were stabilized 15 min at the desired temperature before measuring. The data acquisition was done with the ALV-Correlator Control software and the analysis time was fixed for each sample at 120 s. All vesicles solutions were prepared in 10 mM Tris buffer at pH 7.4.

DSC. Differential scanning calorimetry analyses were performed on a TA Instruments Q100 apparatus at a rate of 10 °C min^{-1}, under continuous flow of nitrogen and helium (25 mL min^{-1}), using sealed aluminium capsules. The thermograms were recorded according to the following cycles: −50 to +100 °C at 10 °C min^{-1}; +100 to −50 °C at 10 °C min^{-1}; −50 °C to +100 °C at 10 °C min^{-1}.

μDSC. Thermograms were recorded on a MicroDSCIII Evo Type Tian-Calvet calorimeter from Setaram. Analyses were performed on 0.8 mL of a 10 mg mL^{-1} vesicle solution introduced in a standard cell. Solution was first stabilized in calorimeter for 3 h at 5 °C. Two heating and one cooling scans were then recorded at 0.5 °C min^{-1} from 5 °C to 55 °C with 15 min isotherms at 55 and 5 °C.

Fluorescence spectroscopy measurements. For fluorescence measurements, a Varian Cary Eclipse fluorescence spectrophotometer was used. Temperature in a 1 cm glass cell was regulated with a Peltier-thermostated cell holder and decantation hindered by electromagnetic stirring in the cell. Stock solutions of laurdan were made in DMSO. Copolymer/laurdan dispersions were made with a copolymer/probe ratio of 125 : 1 (laurdan final concentration was 2 μM) by adding a concentrated drop of laurdan in DMSO onto preformed vesicles. Excitation wavelength was set at 350 nm and emission scans recorded from 380 to 500 nm with slow scan speeds for best S/N ratio. Excitation and emission filter slits were held at 5 nm.

Refractive index increment. Values of dn/dc were determined independently for each temperature with a differential refractometer operating at 658 nm (Optilab rEX, Wyatt). Five solutions, a parent solution and four dilutions, were analyzed to determine each value of dn/dc. The first derivative of the dn/dc variation according to temperature was plotted.

Transmission electron microscopy. TEM images were recorded on a Hitachi H7650 microscope working at 80 kV equipped with a GATAN Orius 11 Megapixel camera. Samples were prepared by spraying a 1 g L^{-1} solution of the block copolymer onto a copper grid (200 mesh coated with carbon) using a homemade tool.

Optical microscopy. Visible and fluorescence microscopy images were taken on a Zeiss Axiovert 40 CFL inverted microscope. For fluorescence, a Hg lamp and Nikon DAPI-FITC-Texas Red excitation filter with narrow bandpass windows in the violet (395 to 410 nm), blue (490 to 505 nm) and green (560 to 580 nm) spectral regions were used. Vesicles were imaged between glass plate and coverslip separated with a thin silicon CAF 4 layer preventing compression of the vesicles.

III. Results and discussion

In a previous work, we demonstrated the self-assembly properties of the amphiphilic $PTMC_{22}$-*b*-PGA_{14} copolymer in aqueous solutions. This block copolymer forms vesicular assemblies whose sizes might be adjusted by varying the conditions of preparation. In a nanoprecipitation approach, these conditions were among others the choice of the organic solvent, the concentration of copolymer, the order of addition (water in organic solvent or the opposite) and the injection flow rate.[37] PTMC-*b*-PGA vesicles displayed a typical double layer membrane made of interdigitated hydrophobic PTMC blocks stabilized by hydrophilic PGA blocks on either side of the PTMC layer.

PTMC is known as an amorphous polymer. However, it has been demonstrated that relatively short PTMC chains ($M \sim < 10\,000$ g mol^{-1}) may crystallize in some conditions.[39,40] Here, the molecular weight of the PTMC block being far lower than this threshold, it is expected that some crystallinity is preserved in the membrane of PTMC-*b*-PGA vesicles at room temperature. This should strongly influence the physicochemical behaviour of the polymersomes dispersed in aqueous solutions. Herein, the purpose of the work is to evaluate the influence of the crystallization/melting process on the polymersome stability and to compare it with temperature behavior of liposomes.

A. Evidence of PTMC crystallization in polymersomes

Thermal properties of bulk $PTMC_{22}$ homopolymer and $PTMC_{22}$-*b*-PGA_{14} diblock copolymer have been studied by DSC. PTMC having molecular weight between 1000 and 12 000 g mol^{-1} is known to crystallize with a melting temperature (T_m) close to body temperature.[39,40] In Fig. 1A, which represents results during first heating scan, the peak melting temperature of $PTMC_{22}$ homopolymer (M_n = 2250 g mol^{-1}) and $PTMC_{22}$-*b*-PGA_{14} copolymer are comprised between 36 and 37 °C with corresponding enthalpies of 7.8 and 13.5 J g^{-1} (Table 2). This increase in melting enthalpy probably arose from microphase separation in the bulk copolymer, inducing a confinement of the PTMC chains that favoured their crystallization. Furthermore,

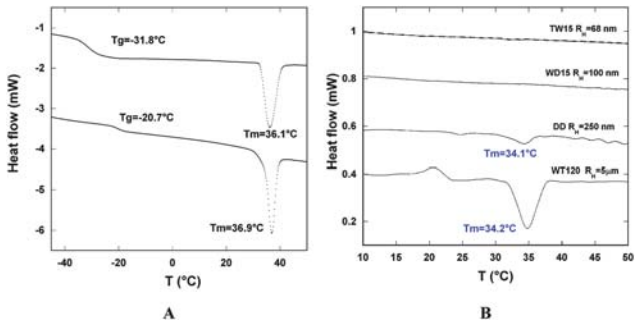

Fig. 1 (A) DSC thermograms of $PTMC_{22}$ (up) and $PTMC_{22}$-*b*-PGA_{14} (down) in bulk during first heating scan (10 °C min^{-1}). (B) µDSC thermograms of $PTMC_{22}$-*b*-PGA_{14} vesicles observed during the first heating scan at 0.5 °C min^{-1} after a 3 h isotherm at 5 °C ([copolymer] = 10 mg mL^{-1}). See Table 1 for methods of preparation of polymersomes. DD stands for direct dissolution.

the glass transition temperature (T_g) increases from −32 °C in the homopolymer to −21 °C in the copolymer due to decreased mobility of the chains caused by microphase separation. In addition, it has to be noted that, as low molecular weight PTMC crystallizes slowly, no melting transition could be observed in the second DSC heating run when temperature was increased from −50 °C to 100 °C.

Thermograms of 1% (w/v) vesicular solutions with different sizes, as prepared by nanoprecipitation, were then recorded by microcalorimetry experiments (Fig. 1B). No melting peaks were detected for small vesicles having average hydrodynamic radii below 100 nm. These batches were prepared from two different organic solvents namely THF–MeOH (TW15) and DMSO (WD15) to prove that membrane fluidization by eventual traces of remaining DMSO is not the factor preventing the PTMC crystallization. By increasing the size of the vesicles (DD; R_H = 250 nm and WT120-10 mg mL^{-1}; R_H = 5 µm), a melting transition around 34–35 °C can be observed. This melting transition, in the same temperature range as the one observed for $PTMC_{22}$ homopolymer and $PTMC_{22}$-*b*-PGA_{14} diblock copolymer in the bulk, is in agreement with the formation of polymersomes with a semi-crystalline PTMC membrane.

Moreover, the melting enthalpy value from the 5 µm size vesicles was close to that of bulk $PTMC_{22}$-*b*-PGA_{14} copolymer (Table 2). This suggested that the degree of crystallinity is comparable, meaning that PTMC blocks are not constrained in these large vesicles. Oppositely, the 240 nm vesicles (DD), even if still crystalline, presented a four times lower melting enthalpy, certainly related to the higher curvature of the membrane that hindered the crystallization process. In addition, the kinetics of crystallization might also play a significant role. Indeed, even if 3 h isotherm at 5 °C that preceded the first heating run was sufficient to reach equilibrium for small vesicles, the small exothermic peak observed around 20 °C for 5 µm vesicles upon heating, clearly showed that some of the sample did not get time to fully crystallize under these conditions.

A better understanding about this mechanism may be achieved by comparison with liposomes. Especially, the phase behaviour of dipalmitoyl phosphatidylcholine (containing 16 carbons acyl chains named C(16)PC hereafter) is now well understood.[41,42] Acyl chains of phospholipids forming liposomes can reside in the membrane in two different main phases: the highly ordered gel state and the less ordered liquid crystalline state. The temperature at which the system, largely cooperatively, changes from the gel to the liquid crystalline phase is called the main phase transition temperature (T_m). So, T_m is an important physical parameter that characterizes the state of aggregation of phospholipids in vesicles.[43] In small vesicles, where bilayer curvature is high, the packing of the phospholipid hydrocarbon chains is less important in comparison to large vesicles where the surface is locally more planar. Hence the formation of an organized (*i.e.* gel phase) in the membrane of small vesicles can be hindered.[44,45] As a consequence, the melting enthalpy corresponding to the main phase transition temperature (T_m) in membrane has been shown to decrease with liposomes size.[46] The same influence of the polymersome size on the transition has been observed with a decrease of the melting enthalpy from 13.2 J g^{-1} to 2.7 J g^{-1} when vesicle radius was decreased from 5 µm to 250 nm respectively (Table 2), resulting from a frustration effect due to increased curvature.

On Fig. 2, the melting of PTMC chains in polymersome bilayers (WT120-10 mg mL^{-1}, R_H = 5 µm) was imaged by polarized optical microscopy. After storage during one night at 5 °C, vesicles were first observed at 25 °C and a clear

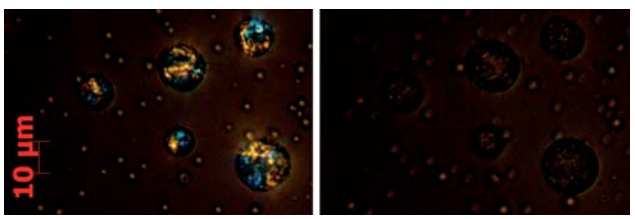

Fig. 2 Disappearance of birefringence observed with optical microscopy under polarized light. WT120-10 mg mL^{-1} vesicles are heated from 25 °C (left) to 40 °C (right).

Table 2 Comparison of melting transitions of bulk homopolymer and copolymer with vesicular aqueous dispersions of different sizes. Values are recorded in the first heating run

Sample code	R_H/nm	PI[a]	Crystallinity	Melting enthalpy (J g^{-1}[b]
TW15	56	0.19	N	—
WD15	95	0.03	N	—
DD	240	0.35	Y	2.7
WT120–10 mg ml^{-1}	5000	0.4	Y	13.2
$PTMC_{22}$ (block)			Y	7.8
$PTMC_{22}$-*b*-PGA_{14} (block)			Y	13.5

[a] Polydispersity index determined by dynamic light scattering. [b] Calculated as per mass of PTMC for comparison.

birefringence could be observed, attesting the presence of crystalline domains in vesicles. However, when heated up to 40 °C, this birefringence disappeared after 30 s, in agreement with a melting transition.

B. Consequence of PTMC crystallization/melting on vesicle size

In the previous part, a clear analogy has been established between the melting of PTMC polymeric chains in $PTMC_{22}$-*b*-PGA_{14} vesicles and the gel-to-liquid crystalline phase transition in liposomes. We were then interested to describe how this transition can influence the overall size of the vesicles and what would be the transition mechanism. For this purpose, dynamic light scattering (DLS) experiments as a function of temperature from vesicles with different sizes, ranging from 100 nm to 500 nm in R_H, were conducted (Fig. 3). However, the giant vesicles (WT120-10 mg mL^{-1}, $R_H = 5$ μm) have not been studied by DLS (due to their too large dimensions to have relevant DLS data). A remarkable decrease in vesicle size was observed upon heating above the melting transition (34–35 °C) for vesicles with hydrodynamic radii of 500 nm and 280 nm. Cooling down to 20 °C resulted in turning back to the initial size indicating the reversible nature of the process. Moreover, the heating and cooling runs presented an hysteresis which was a prominent feature of any system undergoing a first-order phase transition, as already mentioned in both experimental[28,47] and computational work[48,49] on lipidic bilayers. Interestingly, when the size of vesicles obtained after direct dissolution (R_H = 250 nm; PDI = 0.4) was reduced by extrusion (R_H = 150 nm, PDI = 0.16), they were no longer sensitive to temperature variations. Absence of size changes with temperature for small vesicles was confirmed for WD15 vesicles (R_H = 110 nm) during heating/cooling cycles (Fig. 3).

Contin analysis was also used to obtain a better insight about the size variation and its distribution with temperature.

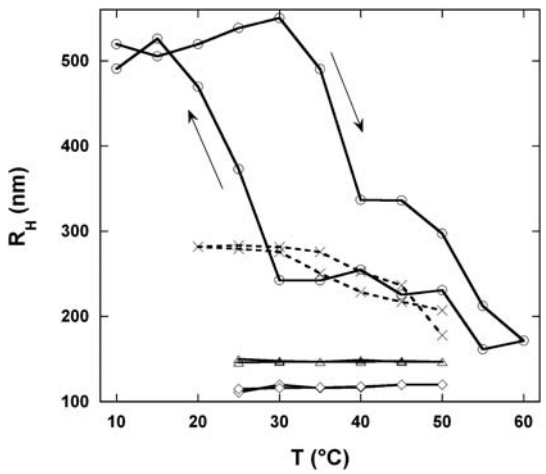

Fig. 3 Dynamic light scattering study of $PTMC_{22}$-*b*-PGA_{14} vesicle sizes with temperature. Temperature was increased by 5 °C steps and kept constant for 15 min at each temperature. Time relaxation curves were fitted with a monoexponential function. (○: WT120-1 mg mL^{-1}; ×: direct dissolution; Δ: direct dissolution and extrusion through 0.2 μm membrane filter; ◇: WD15). Polymer concentration was set at 1 mg mL^{-1}.

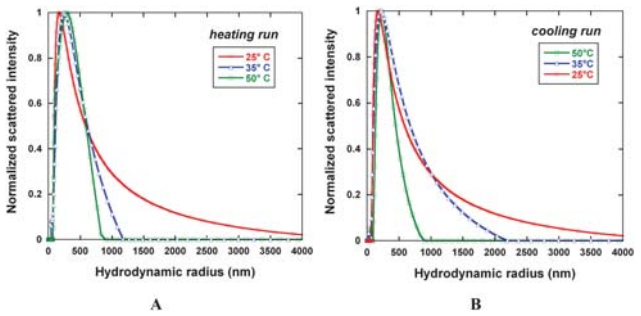

Fig. 4 DLS in Contin mode of vesicles prepared by direct dissolution and submitted to a temperature (A) heating and (B) cooling cycle between 25 °C and 50 °C (15 min per temperature). For clarity, only curves at 25 °C (○), 35 °C (△) and 50 °C (□) are represented.

Noteworthy, only one population of vesicles was recorded during heating–cooling cycles. This indicated that the evolution of the observed vesicles through particle enlargement/size reduction did not imply secondary aggregation phenomenon. For instance, we detailed on Fig. 4 the size distribution of vesicles obtained by direct dissolution which covered a broad size range (PDI = 0.4). The results revealed that the largest vesicles progressively disappeared by increasing temperature. At 25 °C vesicles radii were ranging from 80 nm to 4 μm, whereas at 50 °C the largest vesicles have a radius of 800 nm only. These data also confirmed the highest sensitivity of large vesicles towards temperature variations, as described on Fig. 3.

The mean light scattered intensity has also been measured as a function of temperature (Fig. 5A). The intercept between the two regimes gave an estimation of the transition temperature around 35 °C, in the same range of the melting transition determined from microcalorimetry experiments. This basic measurement has shown a high sensitivity and reliability for the determination of the main phase transition temperature in liposomes. Its variation with temperature arises mainly from the refractive index variation of the lipidic membrane between gel and liquid crystalline phase.[50] In our case, the refractive index increment (dn/dc) variation of vesicle solution showed a maximum around 32 °C (Fig. 5B).[51] As a result, the observed mean light scattered intensity variation were the consequence both of the change of the membrane structure depicted by the refractive index variation and of the size variation of vesicles shown in Fig. 3.

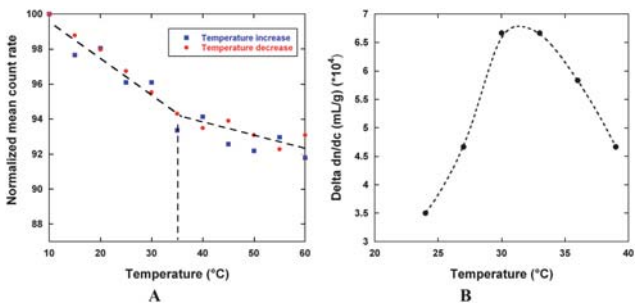

Fig. 5 Evolution of (A) the mean count rate scattered intensity and (B) the derivative of the refractive index increment (dn/dc) with temperature for WT120-1 mg mL^{-1} (R_H = 450 nm).

C. Polymersome size transition mechanism

In order to better elucidate the origin of the size transition observed in $PTMC_{22}$-*b*-PGA_{14} polymersomes, analogies with liposomes made of crystallizable lipids can be performed. Indeed, the influence of main phase transition upon cooling on the overall increase of liposomes size is well understood, and explained as a spontaneous fusion into larger single lamellar vesicles.[44,47,52–54] Membrane fusion is promoted by defects created in the bilayer due to the vicinity of lipid phase transition, lateral phase separation or domain generation, or high local membrane curvature. The prerequisites for fusion are of course membrane proximity but also a high defect density in the adjacent bilayers.[55] Thus temperature can serve as an indirect fusion promotor mainly by increasing the defect density in the membranes by lateral phase separation (*i.e.* presence of boundaries between gel and liquid crystal phases).[28,55,56] In addition, shape transformations in liposomes like budding and fission have also been extensively studied, and the understanding of these phenomenon have been improved through fruitful interactions between theory and experiment.[57,58] Budding and fission arise from a complex interplay between temperature, local curvature and local composition. This phenomenon is common in synthetic vesicle above the melting chain transition. Indeed, as stated above, lateral heterogeneities, leading to the existence of domains in the membrane, can exist in the lipid bilayer due to mixtures of lipids or to phase separation (*i.e.* gel and liquid crystalline patches) induced by temperature variation.[59] When this heterogeneous membrane undergoes a temperature increase, differences in thermal expansivities of the different membrane domains, as well as an increase in energy of the domain boundaries, will drive the system to expel domains (budding and fission).[60–62] Therefore, the average size of the liposomes can be decreased with a budding/fission mechanism by heating above T_m. Oppositely, the average size can be increased by a fusion mechanism upon cooling down below T_m.

Both size and shape variations of $PTMC_{22}$-*b*-PGA_{14} giant vesicles (WT120-10 mg mL^{-1}, $R_H = 5$ μm) have been followed by optical microscopy (Fig. 6) upon heating and cooling. Small buds protruding from vesicles appeared after having set the temperature at 45 °C (Fig. 6A). Interestingly, vesicles did not appear spherical, and facets and edges could be observed. By gently shaking the glass plate at 60 °C a shape transformation occurred with the apparition of vesicles at different stages of fission (Fig. 6B). This gentle shaking probably just allowed the vesicles to desorb from the surface of the glass plate and had no effects on the fission mechanism itself.[63] The logical consequence of these budding/fission events, above the PTMC melting temperature, was a decrease of the overall size of the vesicles as previously described by DLS (Fig. 3).

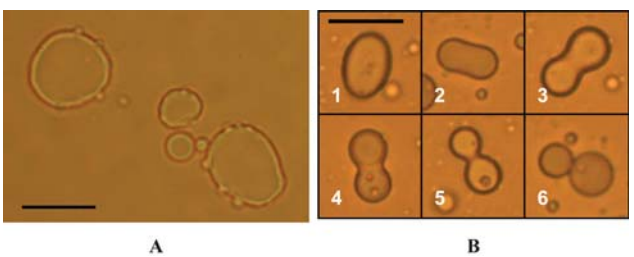

Fig. 6 Optical microscopy observation of $PTMC_{22}$-*b*-PGA_{14} vesicles (WT120–10 mg mL^{-1}). (A) Budding at 45 °C. (B) Snapshots of fission events at 60 °C (different fission stages are depicted from 1 to 6) Scale bar: 10 μm.

The reverse mechanism, inducing the increase of the vesicle size by decreasing temperature, has been also studied using optical and fluorescence microscopy (Fig. 7). Three vesicles fusing together can be observed on Fig. 7A. The typical timescale for an entire fusion event was about 10 s. Noteworthy, this whole fusion process was much longer than the characteristic fusion time for liposomes (in the time scale of one second) or biomembranes (in the time scale of milliseconds). After a first step, where membranes were in close contact, vesicles underwent the classical intermediate "8" shape and oblate sphere, when they gradually fused into one single vesicle. This fusion process was observed using fluorescence microscopy (Fig. 7B). Half of the vesicles were labelled with Bodipy FL (green) and the other half with Nile red (red). The two labelled vesicles were then mixed and observed. Using a multiple band pass excitation filter, the entire fusion event could be followed between red and green vesicles when the temperature was decreased from 40 °C to 25 °C, without having recourse to computer imaging treatment.

Block copolymer vesicles exhibiting a reversible change in size involving fusion/fission mechanism have already been reported in the literature. Eisenberg and coworkers indeed studied size variations of PS-*b*-PAA vesicular dispersions induced by varying the solvent composition.[64,65] Fusion, for instance, was explained in terms of the reduction of the interfacial area. In a recent study, real-time morphology changes of polymer vesicles self-assembled from hyperbranched copolymer HBPO-star-PEO (HPBO was an hyperbranched structure of poly(3-ethyl-3-oxetanemethanol)) was also reported by Zhou *et al.* These large vesicles (100 μm diameter), underwent fusion events under ultrasound treatment at 20 °C and the whole fusion process, observed under optical microscopy, lasted about 1.5 min.[66] The proposed driving force was the perturbation induced by sonication which generated defects on the membranes in contact and destabilized the vesicles. Battaglia and coworkers[67] also reported a novel method to control membrane-enclosed structure morphology. By simply adding poly(ethylene oxide) homopolymer to PEO-*b*-PBD polymersome dispersions, fusion between the vesicles can be controlled, the added PEO perturbing the vesicle membranes. In our case, even if the size variation mechanism was similar, the driving force was totally different and only due to the molecular intrinsic properties related to the crystallinity of our copolymer.

In order to further understand the local modification of the membrane properties underlying this transition mechanism, we incorporated laurdan dye into the vesicle membrane. The alteration of laurdan fluorescence emission was then studied as a function of temperature. Indeed, laurdan is known to display an extreme sensitivity to temperature induced phase transitions in liposomes dispersions.[68,69] When inserted in phospholipidic membranes, its emission depends strongly on the physical state of the surrounding lipids in their gel or liquid crystalline phase. This dependence is a direct consequence of the sensitivity of laurdan to the polarity of its environment. At temperatures below the liquid phase transition (gel state), the reorientation of the surrounding water dipoles is slower than the laurdan fluorescence lifetime and the probe emits at high energy frequencies.

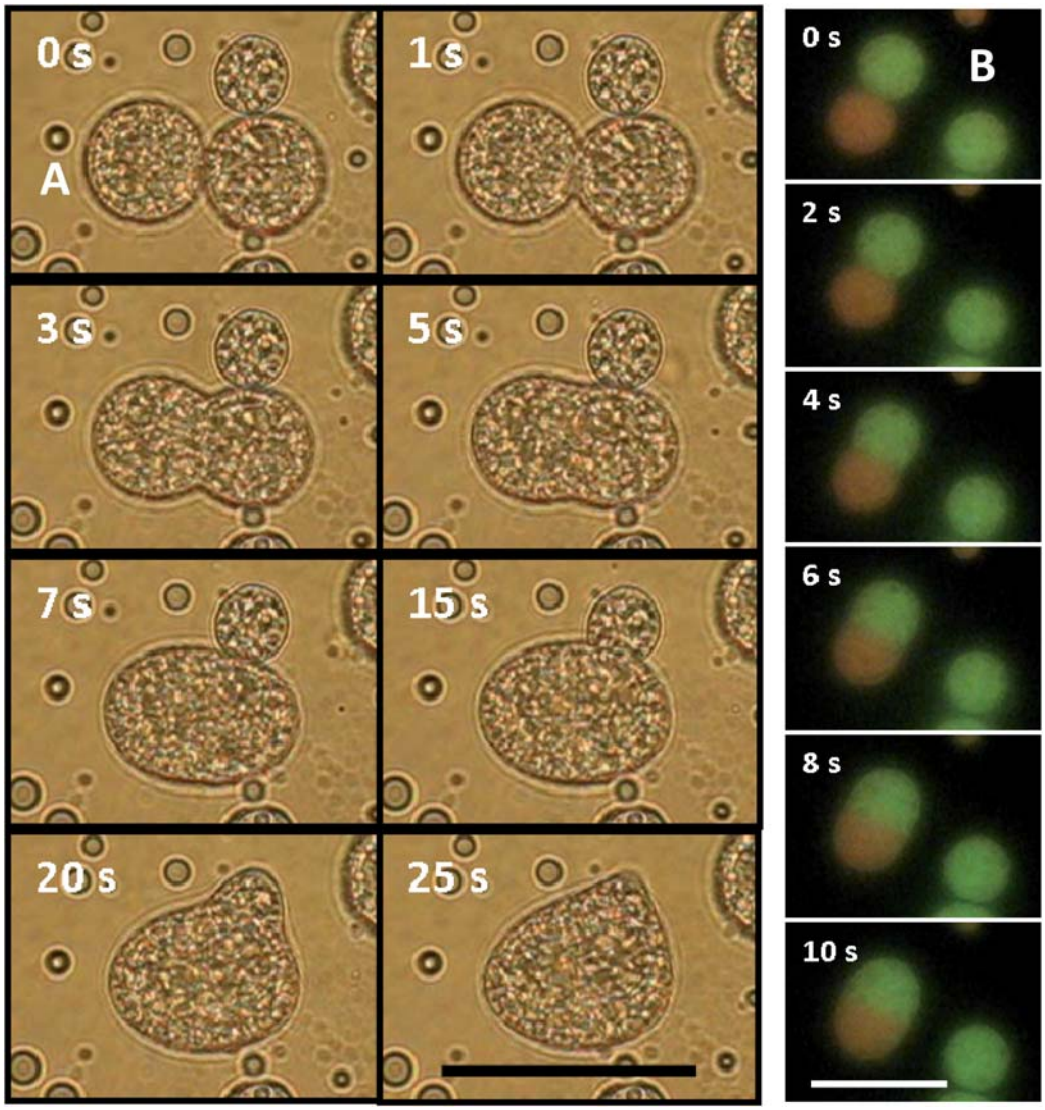

Fig. 7 Snapshots of fusion events observed on $PTMC_{22}$-*b*-PGA_{14} vesicles (WT120-10 mg mL^{-1}) after decreasing temperature from 40 °C to room temperature (A) Optical microscopy. Duration = 25 s. Scale bar 20 μm (B) Fluorescence microscopy. Half of the vesicles were labelled with Nile red and the other half with Bodipy FL. Duration = 10 s. Scale bar 10 μm.

At temperatures above the phase transition (liquid crystalline state) the motion of water dipoles is faster and comparable to the laurdan excited state lifetime and the emission spectrum shifts to lower energy frequencies.[70] Therefore, a good way to quantify the extent of membrane phase separation (*e.g.* lateral heterogeneities between gel and liquid crystal phases) is to use the relationship between the emission intensities obtained below and above the transition temperature. This relationship, called Generalized Polarization (GP) is a useful and accurate indicator of the membrane phase state. In our case, we use the following equation for the calculation of GP

$$GP = \frac{I_{5^\circ C} - I_{60^\circ C}}{I_{5^\circ C} + I_{60^\circ C}} \quad (1)$$

where the temperature below the transition is fixed at 5 °C and the temperature above at 60 °C.[71] Localization of the probe in the membrane was then ascertained using fluorescence microscopy

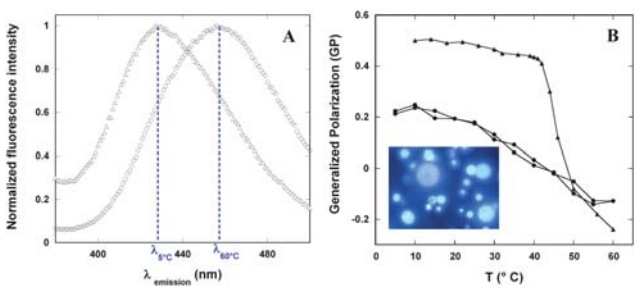

Fig. 8 (A) LAURDAN normalized fluorescence emission spectra in membranes of PTMC-*b*-PGA vesicles at 5 °C (△) and 60 °C (○) with an excitation wavelength of 350 nm. (B) Spectrofluorometric probing of laurdan's generalized polarizability (GP) in (●) PTMC-*b*-PGA vesicles (WT120–10 mg mL^{-1}, R_H = 5 μm) and (▲) DPPC liposomes. Laurdan concentration was set at 2 μM, copolymer/probe ratio was set at 125 : 1.

(insert in Fig. 8-B). Laurdan emission spectrum was then recorded for $PTMC_{22}$-*b*-PGA_{14} vesicles and compared to the one obtained in C(16)PC liposomes.[70] Vesicles were stabilized 15 min at each temperature before measurement. On Fig. 8-A, laurdan emission spectra of polymer vesicles below (5 °C) and above (60 °C) the PTMC melting temperature were presented. Laurdan emission clearly underwent a 30 nm shift with temperature (maximum intensity of 430 nm at 5 °C to 460 nm at 60 °C) which proves that the membrane phase state around the Laurdan fluorescent probes varied. For comparison, laurdan spectral shift in C(16)PC membranes is close to 50 nm.[70]

GP was plotted during heating/cooling temperature cycles. (Fig. 8-B) Interestingly, GP did not exhibit any hysteresis effect during the heating/cooling cycle showing that local reorganization of block copolymer chains in the membrane was rather a fast process (at least less than 15 min) and indicating that membrane phase reached certain equilibrium. The values of laurdan GP in polymersomes at low temperatures were lower than those observed in C(16)PC phospholipids. This traduces a higher hydration around the probe at low temperature and so a less pronounced gel character of the membrane related to the semi-crystallinity of the polymer. On the contrary, above the PTMC melting temperature, GP values were in the range of those obtained in the liquid phase of liposomes which implied that the fluidity of the membranes was similar at high temperatures and that they might be in a comparable liquid disordered fluid state. Transition monitored by GP variation is also less cooperative than in liposome system which reflects the slower chain dynamics due to higher molecular weights.

Lee, Discher and coworkers,[71] using the same GP calculation, observed a constant zero value when laurdan was inserted into polymersome membranes of PEO_{40}-*b*-PEE_{37}. Therefore, PEE being amorphous, no membrane transitions would be expected in this system. As a conclusion, the local membrane modification properties observed here could be directly related to the PTMC crystallization property.

IV. Conclusion

Polymer vesicles of poly(trimethylene carbonate)$_{22}$-*b*-poly(L-glutamic acid)$_{14}$ exhibited in aqueous solution a new type of thermoresponsive behavior affecting their size and stability. This work constituted a proof of concept that vesicular membrane can be affected by the crystalline nature of the hydrophobic block.

PTMC melting temperature was measured at 37 °C in bulk copolymer and around 34 °C in the vesicles with equivalent transition enthalpies. The modification of membrane properties resulting from PTMC conformation change with temperature caused a reversible size variation of the vesicles. The mechanism for this size change, elucidated by dynamic light scattering, optical and fluorescence microscopy, involved fusion and fission/budding of the vesicles.

In this study we have also demonstrated that this transition was strongly dependent on the vesicle size, since neither melting transition nor vesicle size modification was detected for small vesicles. Indeed, high membrane curvature hindered the formation of an ordered crystalline phase.

Since membrane permeability in liposomes is known to be maximum at the gel-to-liquid crystalline transition temperature, the encapsulation and release of a hydrophilic molecule in PTMC-*b*-PGA vesicles should be studied as a function of temperature. This could open new perspectives in controlled drug delivery applications and will be the topic of forthcoming publications.

Acknowledgements

We thank Mr Christian Peronnet and Mr Luc Benoist from Setaram Instrumentation (Caluire, France) for microcalorimetry measurements, as well as the CNRS and Région Aquitaine for Funding (C. Sanson PhD grant).

References

1 F. Ahmed, P. J. Photos and D. E. Discher, *Drug Dev. Res.*, 2006, **67**, 4–14.
2 C. LoPresti, H. Lomas, M. Massignani, T. Smart and G. Battaglia, *J. Mater. Chem.*, 2009, **19**, 3576–3590.
3 H. Aranda-Espinoza, H. Bermudez, F. S. Bates and D. E. Discher, *Phys. Rev. Lett.*, 2001, **87**, 208301.
4 A. Taubert, A. Napoli and W. Meier, *Curr. Opin. Chem. Biol.*, 2004, **8**, 598–603.
5 K. Kita-Tokarczyk, J. Grumelard, T. Haefele and W. Meier, *Polymer*, 2005, **46**, 3540–3563.
6 B. M. Discher, H. Bermudez, D. A. Hammer, D. E. Discher, Y. Y. Won and F. S. Bates, *J. Phys. Chem. B*, 2002, **106**, 2848–2854.
7 F. Chécot, S. Lecommandoux, H. A. Klok and Y. Gnanou, *Eur. Phys. J. E*, 2003, **10**, 25–35.
8 F. Ahmed and D. E. Discher, *J. Controlled Release*, 2004, **96**, 37–53.
9 F. Ahmed, A. Hategan, D. E. Discher and B. M. Discher, *Langmuir*, 2003, **19**, 6505–6511.
10 M. Kumar, M. Grzelakowski, J. Zilles, M. Clark and W. Meier, *Proc. Natl. Acad. Sci. U. S. A.*, 2007, **104**, 20719–20724.
11 W. Meier, C. Nardin and M. Winterhalter, *Angew. Chem., Int. Ed.*, 2000, **39**, 4599–4602.
12 C. Nardin, J. Widmer, M. Winterhalter and M. Meier, *Eur. Phys. J. E*, 2001, **4**, 403–410.
13 M. Sauer, T. Haefele, A. Graff, C. Nardin and W. Meier, *Chem. Commun.*, 2001, 2452–2453.
14 A. Graff, M. Sauer, P. Van Gelder and W. Meier, *Proc. Natl. Acad. Sci. U. S. A.*, 2002, **99**, 5064–5068.
15 D. A. Christian, S. Cai, D. M. Bowen, Y. Kim, J. D. Pajerowski and D. E. Discher, *Eur. J. Pharm. Biopharm.*, 2009, **71**, 463–474.
16 D. H. Levine, P. P. Ghoroghchian, J. Freudenberg, G. Zhang, M. J. Therien, M. I. Greene, D. A. Hammer and R. Murali, *Methods*, 2008, **46**, 25–32.
17 S. Lecommandoux, O. Sandre, F. Chécot and R. Perzynski, *Prog. Solid State Chem.*, 2006, **34**, 171–179.
18 S. Lecommandoux, O. Sandre, F. Chécot, J. Rodriguez-Hernandez and R. Perzynski, *Adv. Mater.*, 2005, **17**, 712–718.
19 S. Lecommandoux, O. Sandre, F. Chécot, J. Rodriguez-Hernandez and R. Perzynski, *J. Magn. Magn. Mater.*, 2006, **300**, 71–74.
20 M.-H. Li and P. Keller, *Soft Matter*, 2009, **5**, 927–937.
21 F. Meng, Z. Zhong and J. Feijen, *Biomacromolecules*, 2009, **10**, 197–209.
22 O. Onaca, R. Enea, D. W. Hughes and W. Meier, *Macromol. Biosci.*, 2009, **9**, 129–139.
23 J. Rodriguez-Hernandez, F. Checot, Y. Gnanou and S. Lecommandoux, *Prog. Polym. Sci.*, 2005, **30**, 691–724.
24 Y. Li, S. L. Brad and L. M. Charles, *Angew. Chem., Int. Ed.*, 2006, **45**, 5792–5795.
25 S. Qin, Y. Geng, D. E. Discher and S. Yang, *Adv. Mater.*, 2006, **18**, 2905–2909.
26 F. Chécot, S. Lecommandoux, Y. Gnanou and H.-A. Klok, *Angew. Chem., Int. Ed.*, 2002, **41**, 1339–1343.
27 H. Iatrou, H. Frielinghaus, S. Hanski, N. Ferderigos, J. Ruokolainen, O. Ikkala, D. Richter, J. Mays and N. Hadjichristidis, *Biomacromolecules*, 2007, **8**, 2173–2181.
28 S. Leekumjorn and A. K. Sum, *Biochim. Biophys. Acta, Biomembr.*, 2007, **1768**, 354–365.

29 W. V. Kraske and D. B. Mountcastle, *Biochim. Biophys. Acta, Biomembr.*, 2001, **1514**, 159–164.
30 D. Volodkin, H. Mohwald, J.-C. Voegel and V. Ball, *J. Controlled Release*, 2007, **117**, 111–120.
31 T.-X. Xiang and B. D. Anderson, *Biochim. Biophys. Acta, Biomembr.*, 1998, **1370**, 64–76.
32 A. P. Gast, P. K. Vinson and K. A. Cogan-Farinas, *Macromolecules*, 1993, **26**, 1774–1776.
33 A. M. Mihut, A. Chiche, M. Drechsler, H. Schmalz, E. D. Cola, G. Krausch and M. Ballauff, *Soft Matter*, 2009, **5**, 208–213.
34 T. Li, W. J. Wang, R. Liu, W. H. Liang, G. F. Zhao, Z. Li, Q. Wu and F. M. Zhu, *Macromolecules*, 2009, **42**, 3804–3810.
35 L. Shen, H. Wang, G. Guerin, C. Wu, I. Manners and M. A. Winnik, *Macromolecules*, 2008, **41**, 4380–4389.
36 P. P. Ghoroghchian, G. Li, D. H. Levine, K. P. Davis, F. S. Bates, D. A. Hammer and M. J. Therien, *Macromolecules*, 2006, **39**, 1673–1675.
37 C. Sanson, J. Le Meins, C. Schatz, A. Brûlet, A. Soum and S. Lecommandoux, *Langmuir*, 2010, **26**, 2751–2760.
38 M. Le Hellaye, N. Fortin, J. Guilloteau, A. Soum, S. Lecommandoux and S. M. Guillaume, *Biomacromolecules*, 2008, **9**, 1924–1933.
39 K. J. Zhu, R. W. Hendren, K. Jensen and C. G. Pitt, *Macromolecules*, 1991, **24**, 1736–1740.
40 Y. Takahashi and R. Kojima, *Macromolecules*, 2003, **36**, 5139–5143.
41 H. Ichimori, T. Hata, H. Matsuki and S. Kaneshina, *Biochim. Biophys. Acta, Biomembr.*, 1998, **1414**, 165–174.
42 R. N. A. H. Lewis, N. Mak and R. N. McElhaney, *Biochemistry*, 1987, **26**, 6118–6126.
43 C. Huang, G. Wang, H. Lin and S. Li, *Biochim. Biophys. Acta, Biomembr.*, 1998, **1373**, 282–288.
44 D. Lichtenberg, E. Freire, C. F. Schmidt, Y. Barenholz, P. L. Felgner and T. E. Thompson, *Biochemistry*, 1981, **20**, 3462–3467.
45 H. J. Risselada and S. J. Marrink, *Soft Matter*, 2009, **5**, 4531–4541.
46 E. Feitosa, P. C. A. Barreleiro and G. Olofsson, *Chem. Phys. Lipids*, 2000, **105**, 201–213.
47 J. Suurkuusk, B. R. Lentz, Y. Barenholz, R. L. Biltonen and T. E. Thompson, *Biochemistry*, 1976, **15**, 1393–1401.
48 S. Leekumjorn and A. K. Sum, *Biochim. Biophys. Acta, Biomembr.*, 2007, **1768**, 354–365.
49 S. J. Marrink, J. Risselada and A. E. Mark, *Chem. Phys. Lipids*, 2005, **135**, 223–244.
50 N. Michel, A.-S. Fabiano, A. Polidori, R. Jack and B. Pucci, *Chem. Phys. Lipids*, 2006, **139**, 11–19.
51 P. N. Yi and R. C. MacDonald, *Chem. Phys. Lipids*, 1973, **11**, 114–134.
52 C. F. Schmidt, D. Lichtenberg and T. E. Thompson, *Biochemistry*, 1981, **20**, 4792–4797.
53 S. E. Schullery, C. F. Schmidt, P. Felgner, T. W. Tillack and T. E. Thompson, *Biochemistry*, 1980, **19**, 3919–3923.
54 M. Wong, F. H. Anthony, T. W. Tillack and T. E. Thompson, *Biochemistry*, 1982, **21**, 4126–4132.
55 G. Cevc and H. Richardsen, *Adv. Drug Delivery Rev.*, 1999, **38**, 207–232.
56 R. C. MacDonald, *Hepatology*, 1990, **12**, 56S–60S.
57 R. Lipowsky, *Nature*, 1991, **349**, 475–481.
58 L. Bagatolli and P. B. S. Kumar, *Soft Matter*, 2009, **5**, 3234–3248.
59 S. Semrau and T. Schmidt, *Soft Matter*, 2009, **5**, 3174–3186.
60 R. Lipowsky, *Curr. Opin. Struct. Biol.*, 1995, **5**, 531–540.
61 H. G. Döbereiner, J. Käs, D. Noppl, I. Sprenger and E. Sackmann, *Biophys. J.*, 1993, **65**, 1396–1403.
62 T. Baumgart, S. T. Hess and W. W. Webb, *Nature*, 2003, **425**, 821–824.
63 W. Wiese, W. Harbicht and W. Helfrich, *J. Phys.: Condens. Matter*, 1992, **4**, 1647.
64 A. Choucair, A. Kycia and A. Eisenberg, *Langmuir*, 2003, **19**, 1001–1008.
65 L. Luo and A. Eisenberg, *Langmuir*, 2001, **17**, 6804–6811.
66 Y. Mai, Y. Zhou and D. Yan, *Macromolecules*, 2005, **38**, 8679–8686.
67 T. Smart, P. C. Fernyhough, A. Ryan and G. Battaglia, *Macromol. Rapid Commun.*, 2008, **29**, 1855–1860.
68 L. A. Bagatolli, *Biochim. Biophys. Acta, Biomembr.*, 2006, **1758**, 1541–1556.
69 T. Parasassi and E. Gratton, *J. Fluoresc.*, 1995, **5**, 59–69.
70 L. A. Bagatolli, B. Maggio, F. Aguilar, C. P. Sotomayor and G. D. Fidelio, *Biochim. Biophys. Acta, Biomembr.*, 1997, **1325**, 80–90.
71 J. C.-M. Lee, H. Bermudez, B. M. Discher, M. A. Sheehan, Y.-Y. Won, F. S. Bates and D. E. Discher, *Biotechnol.Bioeng.*, 2001, **73**, 135–145.

